Novel High Speed Fiber-Optic Pressure Sensor Systems

Prepared by:
Brian Vuksanovich, M.S.M.E., P.E.
Department of Mechanical Engineering Technology
Youngstown State University

Xingwei Wang, Ph.D.
Department of Electrical Engineering
The University Massachusetts, Lowell

Technical Report Documentation Page

1. Report No.	2. Government Accession No.	3. Recipient's Catalog No.
4. Title and Subtitle		5. Report Date
Novel High Speed Fiber-Optic Pressure Sensor Systems		**March 2014**
		6. Performing Organization Code
7. Author(s)		8. Performing Organization Report No.
Brian Vuksanovich and Xingwei Wang		
9. Performing Organization Name and Address		10. Work Unit No. (TRAIS)
Youngstown State University **One University Plaza** **Youngstown, OH 44555**		
		11. Contract or Grant No.
		SJN211353
12. Sponsoring Agency Name and Address		13. Type of Report and Period Covered
Ohio Department of Transportation **1980 West Broad Street** **Columbus, Ohio 43223**		**Final Report**
		14. Sponsoring Agency Code
15. Supplementary Notes		
16. Abstract		
The goal of this project is to develop a complete test of this technology for high-speed, high-accuracy applications, specifically cost-effective data acquisition techniques and practical mounting methods tailored for the subject environment. The secondary goal is to develop improvements to increase pressure capabilities to 500 MPa suggest manufacturing methods for sensor production. The testing will center on the high-speed and high pressure end of the performance envelope as this would provide information that is also useful for the slower and lower pressure applications.		
17. Keywords		18. Distribution Statement
Pressure sensor, high speed, ballistic, fiber optic sensor		**No restrictions. This document is available to the public through the National Technical Information Service, Springfield, Virginia 22161**

19. Security Classification (of this report)	20. Security Classification (of this page)	21. No. of Pages	22. Price
Unclassified	**Unclassified**	**26**	

Form DOT F 1700.7 (8-72)   **Reproduction of completed pages authorized**

Novel High Speed Fiber-Optic Pressure Sensor Systems

Prepared by:
Brian Vuksanovich, M.S.M.E., P.E.
Department of Mechanical Engineering Technology
Youngstown State University

Xingwei Wang, Ph.D.
Department of Electrical Engineering
The University Massachusetts, Lowell

Nan Wu (Postdoctoral researcher)
Yang Zhang (MS student)
Tyler Schmitt (REU student)
Department of Electrical Engineering
The University Massachusetts, Lowell

March 2014

Acknowledgments

Table of Contents

Purpose of the Research

The research centers on the development and characterization of a type of pressure sensor that would provide an alternative to the current industry standard piezoelectric sensors. The current sensors have a limited response time and are subject to electromagnetic interference (EMI). Additionally, they are expensive which limits their use to laboratory settings. A less expensive sensor with improved resistance to environmental effects such as high temperatures, EMI and high pressures would provide opportunities for improvement in areas such as real-time monitoring of internal combustion engines and turbines, manufacturing processes like forging and metal forming. Additionally, critical safety systems such as airbag deployment and aviation ejection seat control could be monitored and recorded.

The Fiber-Optic Sensor

Dr. Xingwei Wang developed a fiber optic sensor for use in medical devices. One of the main advantages was its small size and it used very little power. Since it uses light, it is immune to EMI effects. It was realized that this sensor could be used in other areas if it could withstand high pressures. Interior ballistics was one of the uses cited and a proposed fiber optic pressure transducer based on Fabry-Perot (FP) interferometer principle was developed. The schematic diagram of the transducer structure is shown in Figure 1. The transducer comprises three components: single-mode fiber (SMF), multi-mode fiber (MMF) and a silicon dioxide (SiO_2) diaphragm. The interrogation laser excites on the FP structure and the reflected interference signal propagates back through the SMF. The interference pattern shifts when the pressure applied on the diaphragm varies. By interrogating the interference pattern shift, the change of the pressure can be calculated.
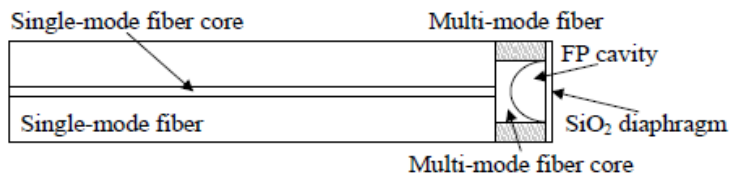
Figure 1. Schematic diagram of fiber optic transducer structure.

Interrogation principle

Light intensity interrogation
In the previous sensor verification experiments, the sensors have demonstrated good linearity, high sensitivity and low hysteresis [16]. However, the interrogation method used in the static experiments was slow. The fiber optic sensor was interrogated by obtaining the reflection interference pattern within a specific wavelength range. By using this interrogation method, the full spectrum of the sensor should be retrieved which makes this method very slow because the capability of processing the huge amount of data in a short time is very limited. In fact, the instrument that was used to interrogate the fiber optic pressure sensor previously sampled data at 5 Hz. It is not fast enough to capture the rapid changing pressure in a shock wave measurement. Therefore, in the blast wave measurement application where a fast interrogation method is needed, the interference pattern interrogation approach is substituted by the light intensity interrogation approach.

2

The principle of the light intensity interrogation approach is illustrated in Figure **2**2. Two plots in the figure demonstrate the interference pattern before the pressure is applied and after the pressure is applied respectively [16]. The dash line indicates the interference pattern after the pressure is applied. Generally, the amount the interference pattern shifts could be calculated by the difference of the valley wavelengths. If a photodetector is used to observe the light intensity at a specific single wavelength, which is referred to "fixed wavelength" in **Figure 2**, as the interference pattern is shifting to the left, the photodetector would observe a light intensity increase. The relationship between the light intensity change and the interference pattern shift is described in the previous literature [20]. Because of the wide bandwidth of the photodetector, the light intensity interrogation method has the capability of tracking fast changing pressures in the blast event by choosing the proper data acquisition (DAQ) system.
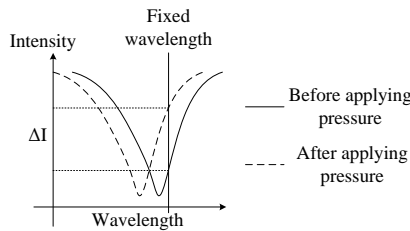
Figure 2. Principle of the light intensity interrogation approach. As the interference pattern shifts, the intensity of the reflection light at a specific fixed wavelength is changed. The amount of the intensity change corresponds to how much the interference pattern shifts.

design and fabrication of transducer

Transducer's structure

Figure 3 shows the schematic diagram of the transducer's structure. The transducer contains a leading single mode fiber (SMF) to transmit optical signals, a short length of multimode (MMF) fiber with etched cavity to form an FP cavity, and a thick diaphragm that is deflected when it is subject to pressure. The incident light reflects at the SMF/MMF and the MMF/diaphragm interfaces. Reflection lights interfere with each other to generate interference pattern, which will be shifted when the FP cavity length is changed due to the pressure variation. Therefore, the pressure can be demodulated through the shift of the interference pattern.
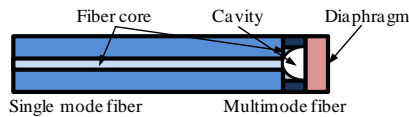
Figure 3. The schematic diagram of the transducer's structure.

Since the diaphragm is the sensing element, it is critical to perform a thorough analysis on the diaphragm to determine its thickness and diameter in order to evaluate the transducer's sensitivity and the dynamic range. The performance of the diaphragm is governed by following formulas [15]:

$$P_{\mathrm{m}} = \frac{8Eh^4}{5(1-\mu^2)(d/2)^4} \cdot \frac{0.145}{1000} \ \text{(psi)}, \tag{1}$$

3

$$Y_c = \frac{3(1-\mu^2)(d/2)^4}{16Eh^3} \cdot 10^9 \cdot \frac{1000}{0.145} \text{ (nm/psi)}, \tag{2}$$

where P_m is the maximum pressure in psi; E is the Young's modulus; μ is the Poisson ratio; h is the thickness of the diaphragm; d is the diameter of the diaphragm; Y_c is the center deflection of the diaphragm under certain pressure. The sensitivity under the current demodulation system (Si720, MicronOptics) is

$$S_{CTS} = 1.55 \times \frac{Y_c}{l} \text{ (nm/psi)}, \tag{3}$$

where l is the FP cavity length in μm.

The maximum pressure can be determined by Eq. (1). However, it is not the range that can be measured because of the demodulation system. It is always expected that the transducer's interference pattern shifts a quarter of the period when it is subject to the desired maximum pressure, which is 100,000 psi in this case. Hence, the dynamic pressure range defines the maximum pressure range that the sensor can measure with the shifting of the interference pattern within a quarter of the period.

The relationship between the phase change of the interference pattern and the Fabry-Perot (FP) cavity length change is:

$$\Delta\phi = \frac{4\pi n \Delta l}{\lambda_0}, \tag{4}$$

where n is the refractive index of the medium inside the FP cavity; λ_0 is the interrogation laser's wavelength in nm. Because only a quarter of the period of the interference spectrum is allowed for the sensor's normal behavior, the maximum of $\Delta\phi$ is a quarter of 2π which is $\pi/2$. Therefore, the maximum Δl is $\lambda_0/8$. By combining this and Eq. (2), the dynamic pressure range can be determined, which is

$$P_d = \frac{\lambda_0}{8Y_c} \text{ (psi)}, \tag{5}$$

Transducer's Fabrication

Figure 4 shows the fabrication process of the fiber optic pressure transducer.

A MMF is spliced with a SMF.

The MMF is cleaved to leave a short length.

The MMF is etched in hydrofluoric acid to form the air cavity.

Another MMF is spliced onto the end face of cavity.

The MMF is cleaved to leave about 30 μm as the diaphragm.
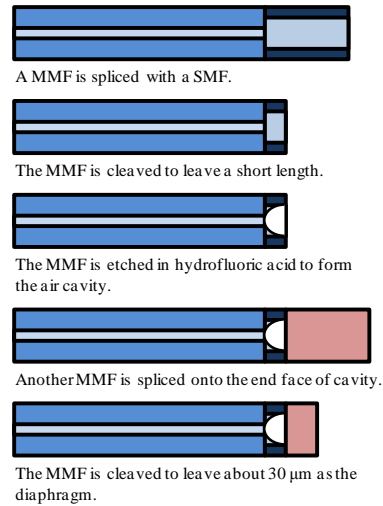
Figure 4: The fabrication process.

A piece of SMF was spliced with a piece of MMF which is cleaved afterwards to leave a short length (~50 μm). The MMF was immersed in 48% hydrofluoric acid to etch away the core to form an air cavity. Another piece of MMF was spliced on the end face of the cavity and then was cleaved to form a thick diaphragm. The thickness was controlled at around 30 μm. Figure 3 shows a microscopic photo of a fabricated transducer.

Figure 5: Microscopic photo of a fabricated fiber optic transducer.

Transducer's package

A metallic package was designed and fabricated to protect transducers and to mount transducer onto the test facility in Benét Labs, as shown in Fig. 6.
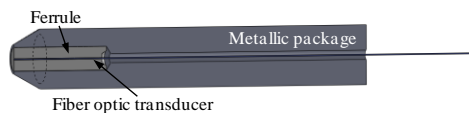
Figure 6: The schematic diagram of the metallic package for the transducer.

A ferrule was attached outside the fiber optic transducer and then the ferrule with the transducer is inserted into the metallic package. Epoxy was used to fix the ferrule and the metallic package. Threads were fabricated outside the metallic package for the mounting purpose. Figure 5 shows a photo of a packaged transducer.

Figure 7: The photo of a packaged transducer

Testing Apparatus

The testing of the sensor was conducted in the Ballistics Laboratory at Youngstown State University. The following equipment was used:

- Enclosed range with 25' drift tube
- (2) PCB 109C11 reference sensors
- 482C05 PCB signal conditioner with unity gain
- Pressure test barrel with (2) ports for the reference sensors and (2) ports for the experimental sensors
- National Instruments USB-6366 DAQ
- xCitex MiDAS DA software for data acquisition
- Physics Applications Fire Control with electronic trigger
- CED Millenium 2 chronographs
- Desktop computer: Intel XeonCPU X5650 @ 2.67 GHz, 6GB RAM, Windows 7 (64bit)
- New Focus Venturi Tunable Laser Source TLB-6600
- ThorLabs PDA10CS InGaAs Amplified Detector
- Optical Sensing Analyser by Micron Optics SI-720
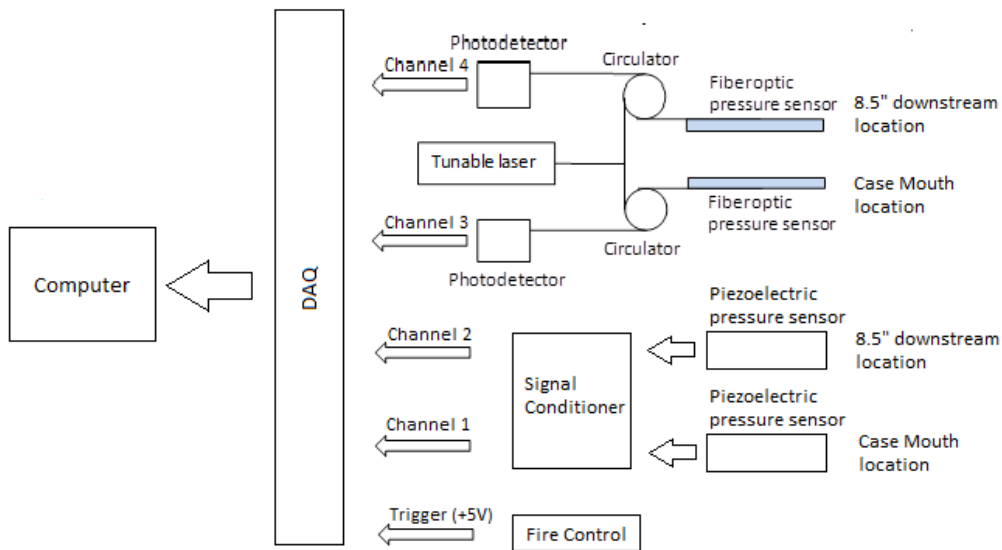
Figure 8: Test Equipment Block Diagram
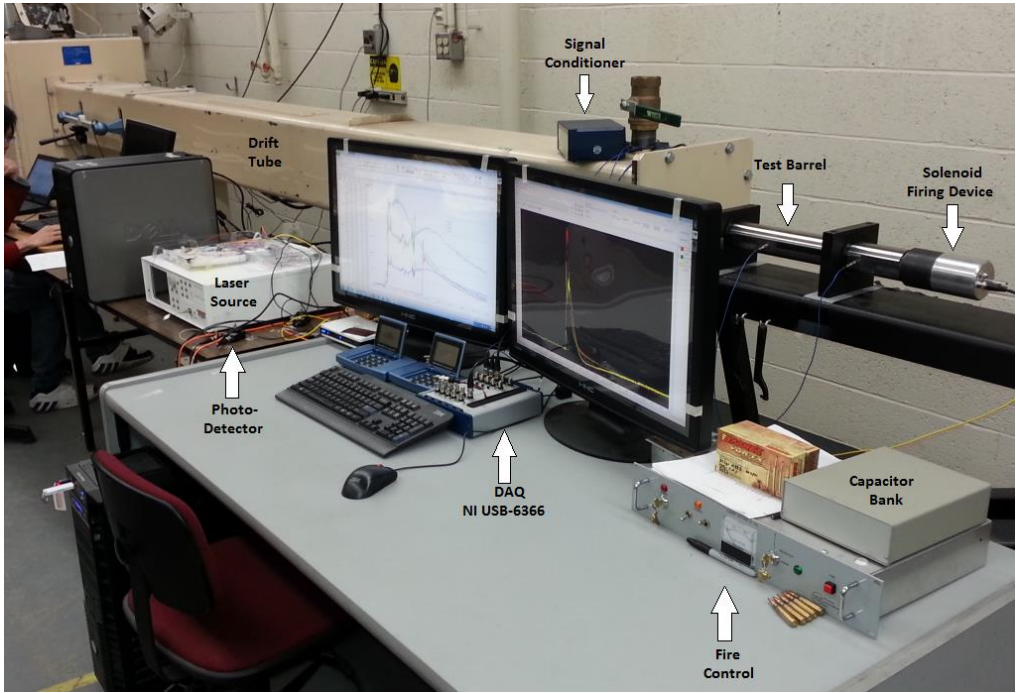
Figure 9: Lab Arrangement
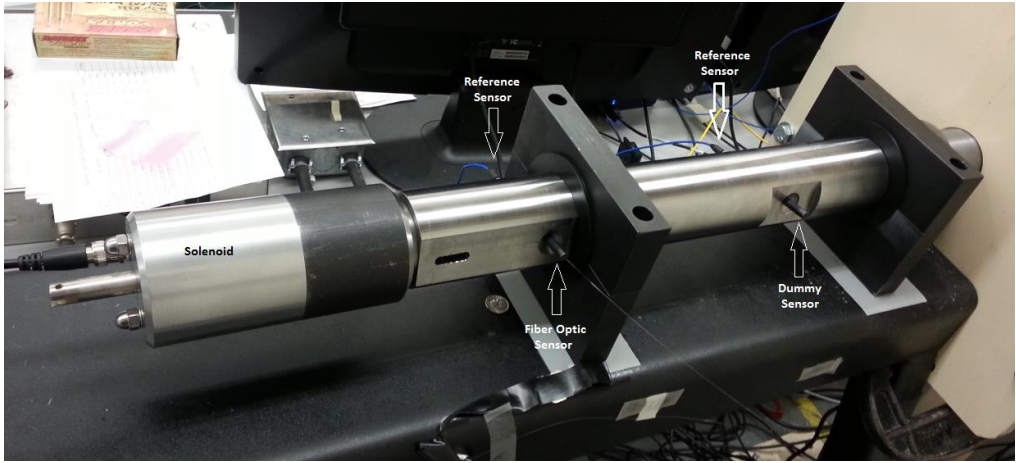
Figure 10: Test Barrel Arrangement

Test Barrel

The barrel is 2.5" O.D., 4140 and was single-point cut-rifled. The test ports were configured to accommodate both the reference sensors and the test sensors at the same time so the same blast event could be monitored by both types of sensors. An additional port is shown on the drawing for a case pressure sensor, but this was omitted as there was no analogous fiber sensor.
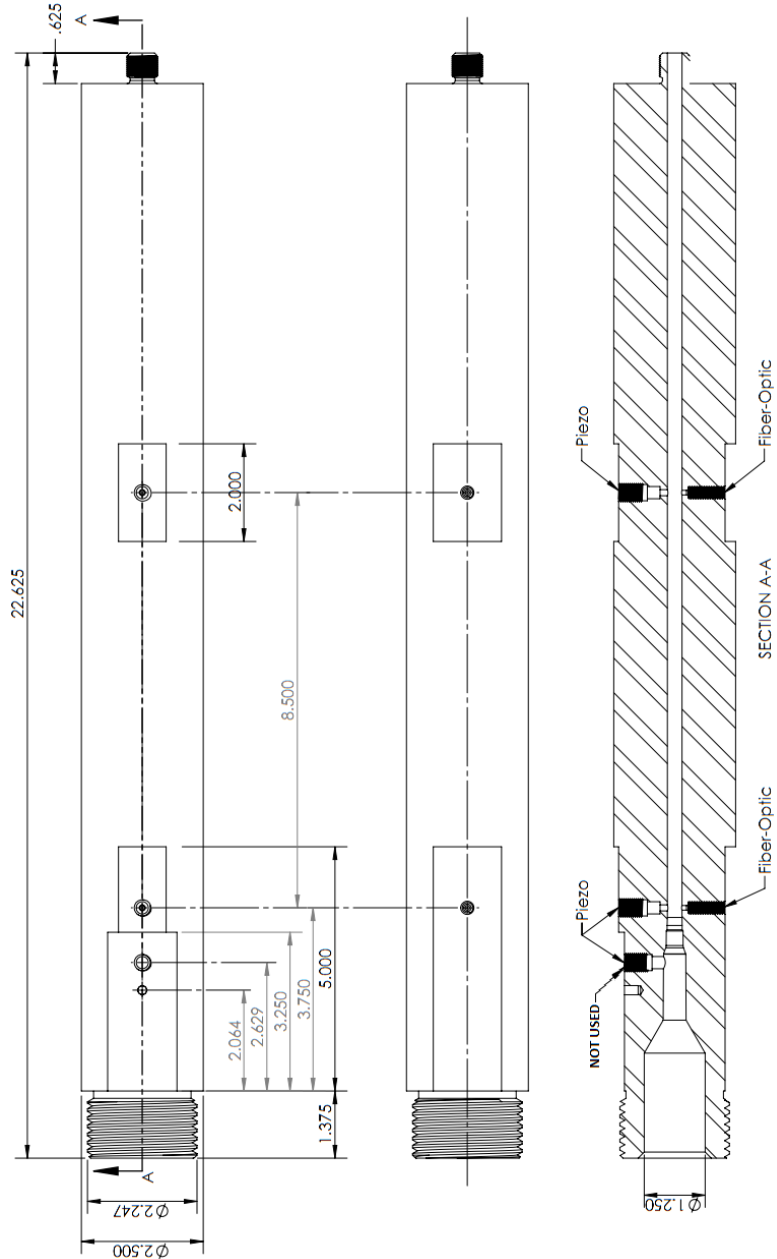
Figure 11: Test Barrel

System Operation

The system operates by firing a 7.62x51mm NATO round down a test barrel equipped with ports to carry the reference sensors and the test sensors. The fire control is a solenoid, screwed onto the chamber end of the barrel, driven by a capacitor bank that supplies the energy to drive a striker into a firing pin to ignite the percussion primer on the round. A +5V signal is also sent when the solenoid is energized to trigger the recording system. The recording system can then be programmed to automatically record a set of data over a time span initiated by the trigger signal.

The barrel is mounted to a 15 foot drift tube that is equipped with two CED Millennium 2 chronographs to record the velocity of the projectile. The bullet passes from the drift tube into an enclosed tank with an impact plate for the projectile to strike. The projectiles used were 150 grain, full metal jacket, lead core. The tank is equipped with a negative pressure air system and is sealed to prevent any spalling or debris from exiting the tank.

The barrel is loaded by removing the solenoid housing and manually placing a round in the barrel chamber. The solenoid housing is then threaded onto the back of the barrel and a striker is placed inside of the solenoid. The system is then ready to fire when the capacitor bank is charged and used to energize the solenoid.

The NI USB-6366 DAQ is connected to the trigger signal from the firing device and to the sensors (through the signal conditioner). This unit was used for all data recording. The data recording was handled by the MiDAS DA DAQ software package and the data exported to Excel for post-processing.

Reference Pressure Data and Reference Sensors

The pressure events used in this characterization are based on the 7.62x51mm NATO cartridge. This provided a well-documented pressure curve with commercially available supplies. Three sample loads were used:

1. M80 Ball (Lake City Manufacture)
    a. 60,000 psi peak pressure
    b. 150gr full-metal jacket projectile
    c. 2,800 ft/s muzzle velocity
2. M80 Reduced Load, Medium Pressure
    a. 36,000 psi peak pressure
    b. 150gr full-metal jacket projectile
    c. 2,300 ft/s muzzle velocity
    d. 36.7gr H335 propellant
3. M80 Reduced Load, Low Pressure
    a. 26,000 psi peak pressure
    b. 150gr full-metal jacket projectile
    c. 2,000 ft/s muzzle velocity
    d. 31.1gr H335 propellant

The M80 ball was procured from ATK and used as delivered. The reduced pressure loads were loaded using Sierra 150gr full-metal jacket projectiles, Barnes Match brass, Winchester Standard Large Rifle

10

Primers and H335 propellant. The powder was measured using an RCBS Chargemaster automatic powder measure and the loading was done on a Dillon 650 press using Dillon carbide dies. All brass was sized with a lubricated sizing die.

The system was checked with the rounds before the testing started to validate that the reference sensors were functioning designed. A PCB representative was present for the test firings. A representative pressure trace is shown below:
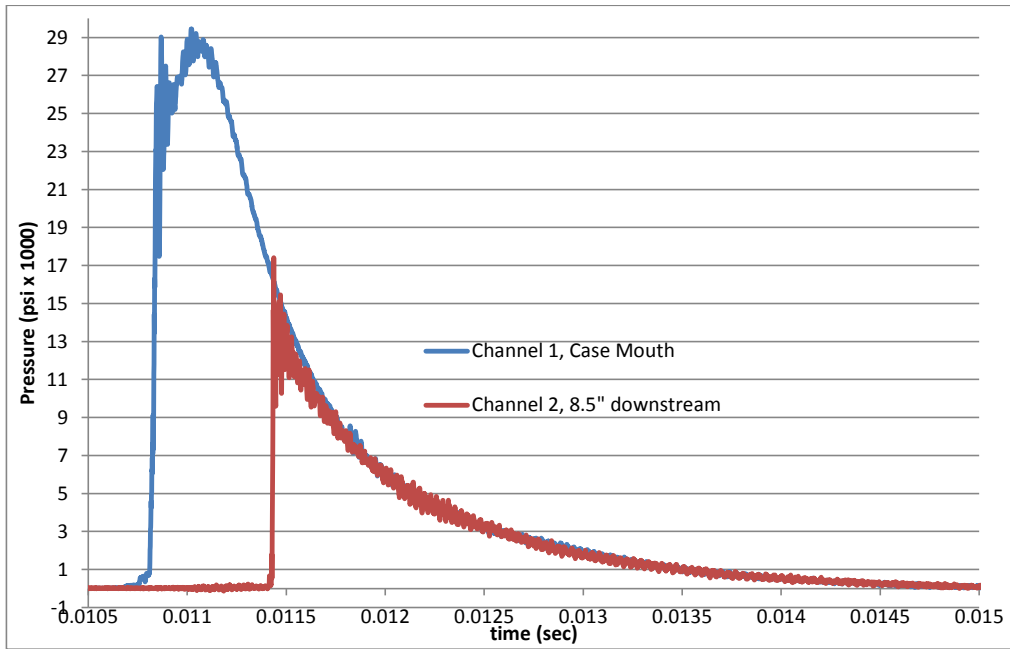
Figure 12: Representative Pressure Trace

Test Results

Five sensors were tested, each sensor having at least three firings with each of the three different pressure loads. Representative traces are shown below:

Sensor025:
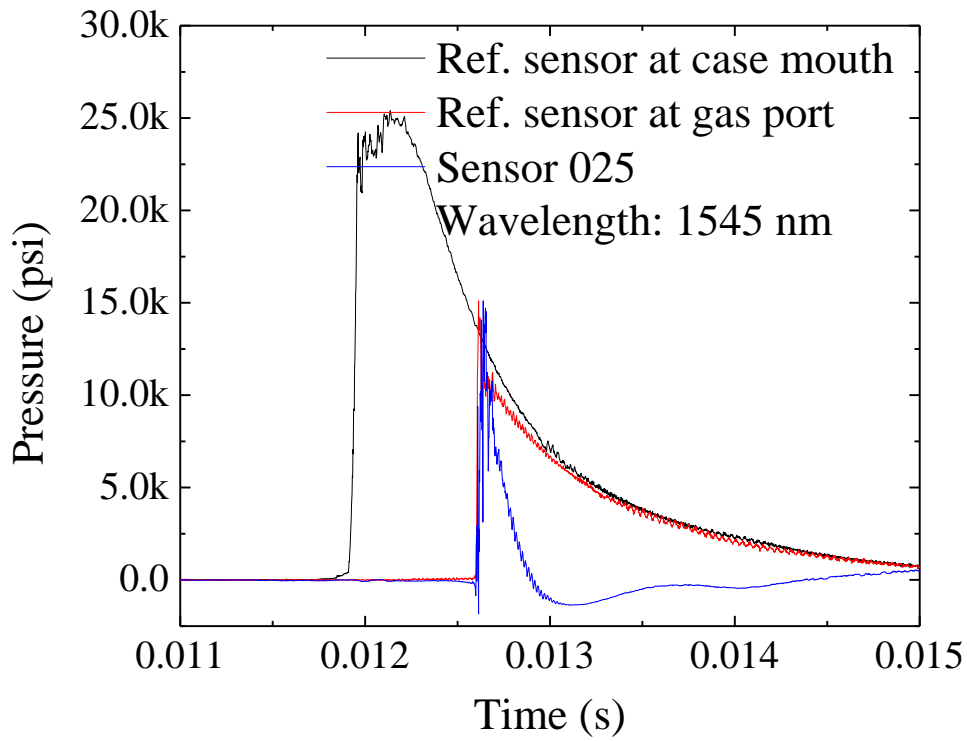
Figure 13: Pressure response from Sensor025 and reference sensors.

The pressure response from Sensor025 when it was mounted at gas port is shown in Fig. 1. Sensor025 showed a faster decay time compared to the other two reference sensors. But it showed the similar ringings to the other two reference sensors during the decay.

Sensor 011:
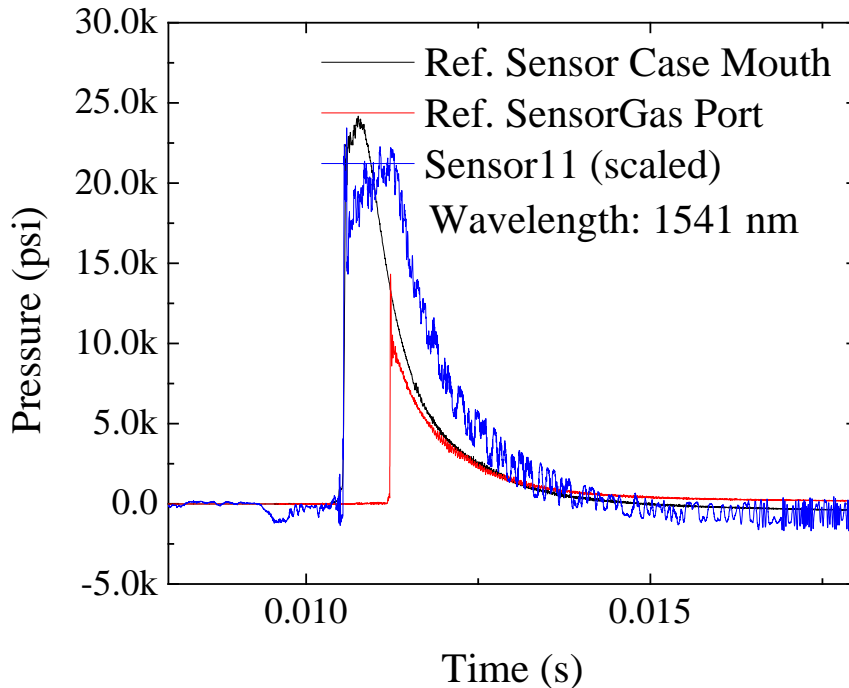
Figure 14: Pressure response from Sensor 11 and reference sensors.

The pressure response from Sensor011 when it was mounted at case mouth is shown in Fig. 2. Unlike Sensor025, Sensor011 showed a longer period at the peak. However, the profile of the pressure captured by Sensor011 is similar to that from the reference sensor. The pressure shown in the figure above is the low pressure generated by H335.

The sensor's response under the high pressure is shown in Fig. 15. It can be seen from the figure that the sensor showed a decrease and then an increase followed by the decay. This is because that the pressure applied on the sensor exceeds its working range, as shown in Fig. 16. Ideally, the sensor should work within the linear range (blue region I) around the working wavelength (1534 nm in this case). Assuming the spectrum shifts right when pressure increases. The optical intensity will increase as the pressure increases. However, if the applied pressure exceeds this region, the optical intensity may go to the red region II in Fig. 16. Thus, although the pressure still increases, the optical intensity from the sensor will decrease. This will cause the over range problem as shown in Fig. 15. However, since the spectrum of the sensor has already been known, the over range part can be compensated. The compensated sensor response is shown in Fig. 17. It can be seen that the signal has been compensated as the pressure increases and decreases.

Comment [x1]: Figure number needs to be fixed.
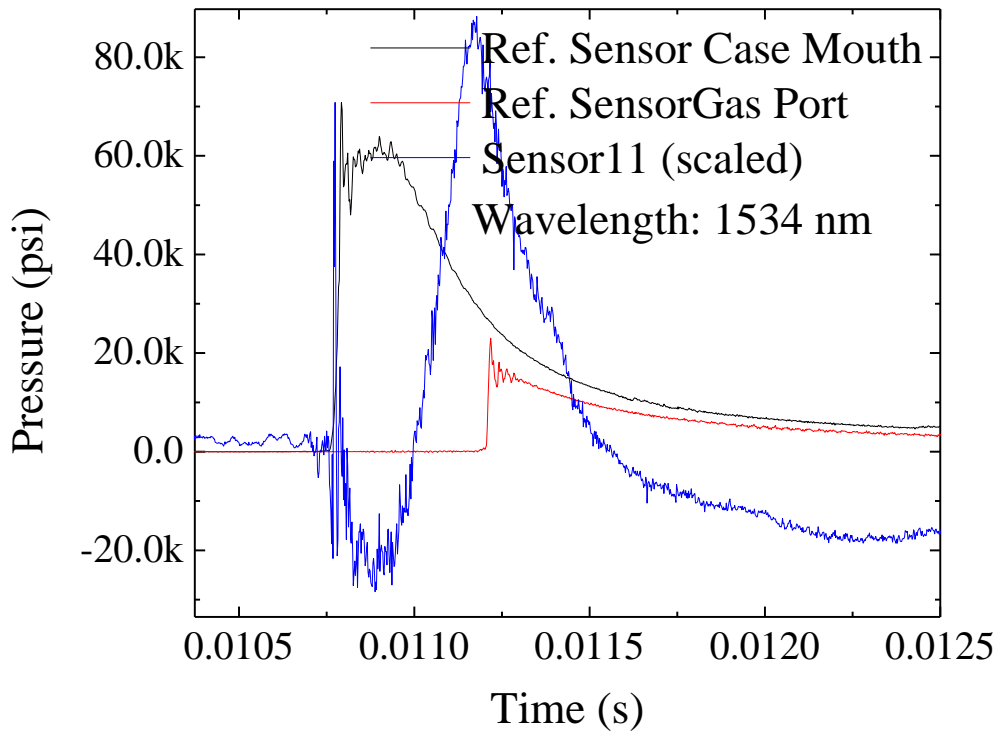
Figure 15: High pressure response from Sensor 11 and reference sensors.
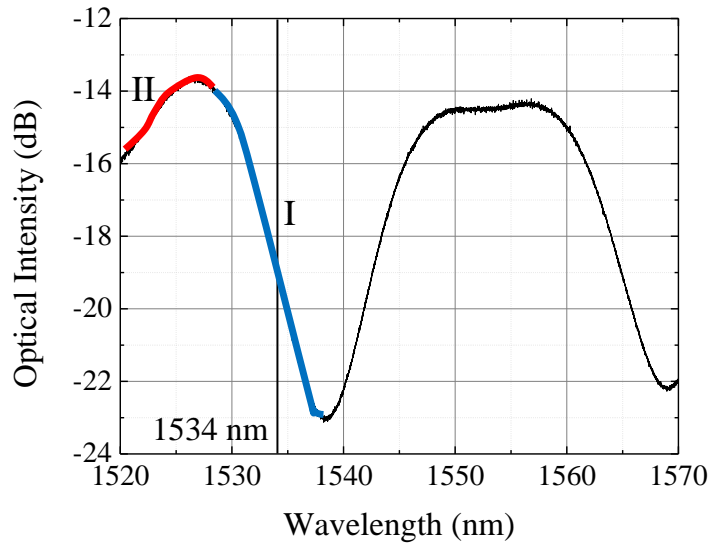
Figure 16: The explanation of Sensor11's response in Figure 15.
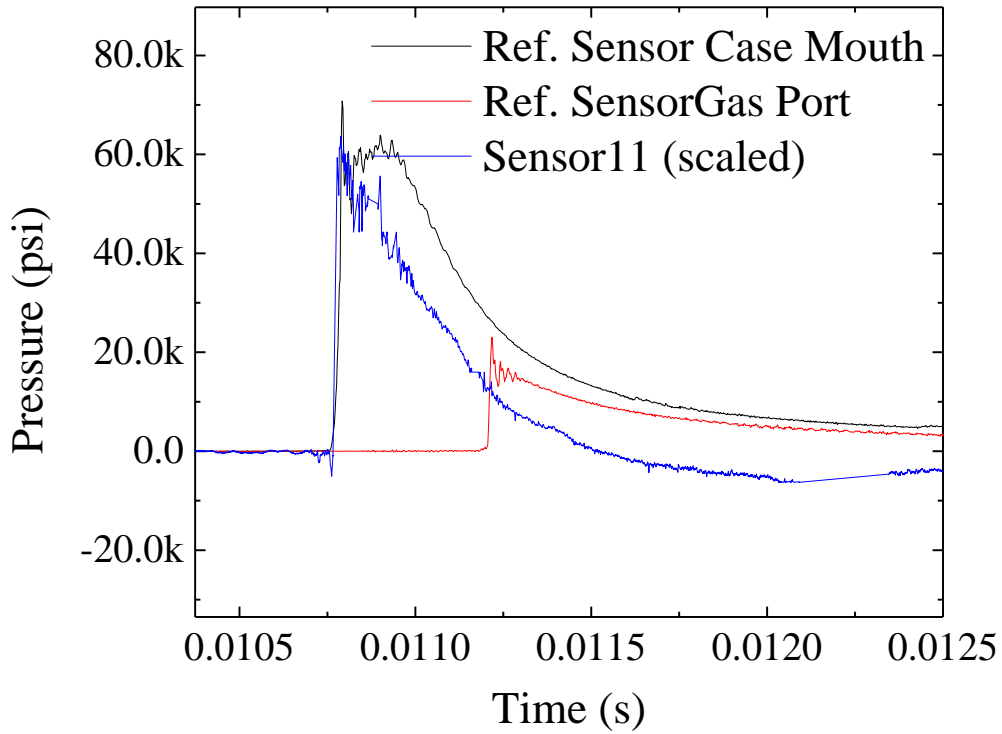
Figure 17: The compensated response from Sensor 11.

The same sensor was subject to the similar pressure (60 kpsi). The original signal and the processed signal are shown in Figure 18.

(a)

(b)
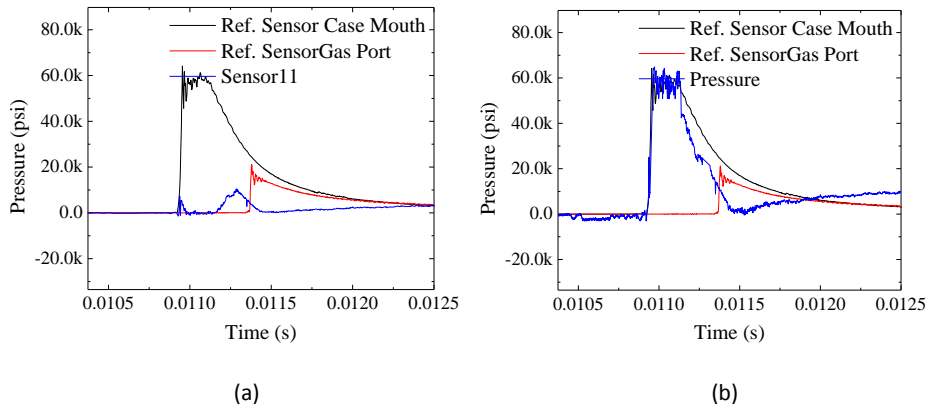
Figure 18: The signal compensation. (a) The original signals. (b) The processed signals.

Sensor 019:
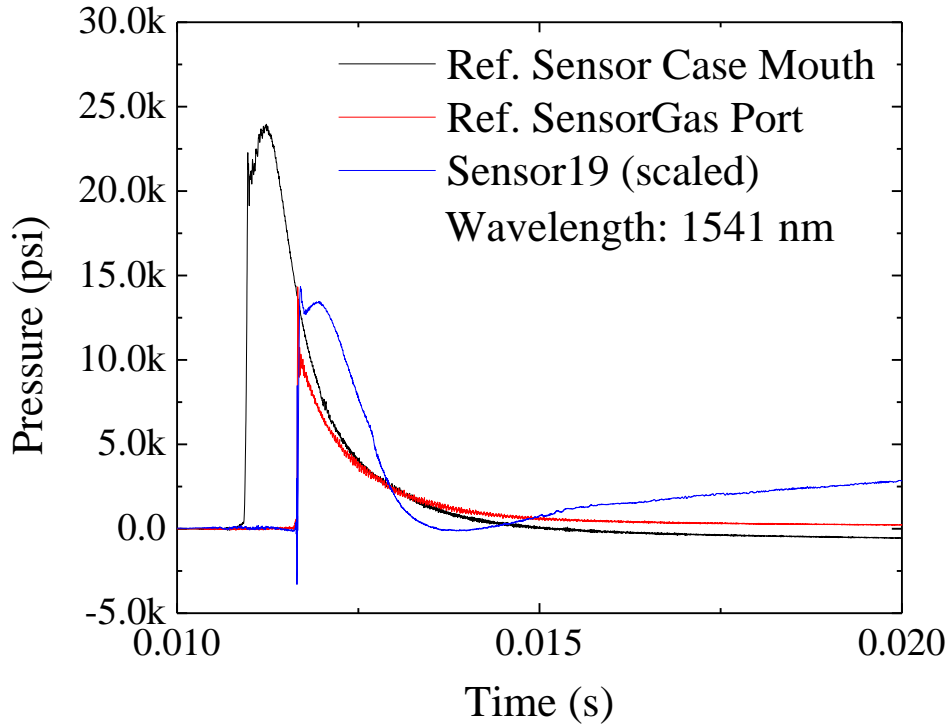
Figure 19: Pressure response from Sensor019 and reference sensors.

The pressure response from Sensor019 is shown in Fig. 19. The sensor was mounted at gas port. It can be seen that the pressure profile follows the profile from the reference sensor. However, after 0.015 s, the response increased. The reason could be that the sensor was leaking. The leakage can be fixed by an improved fabrication process.

Sensor 010:
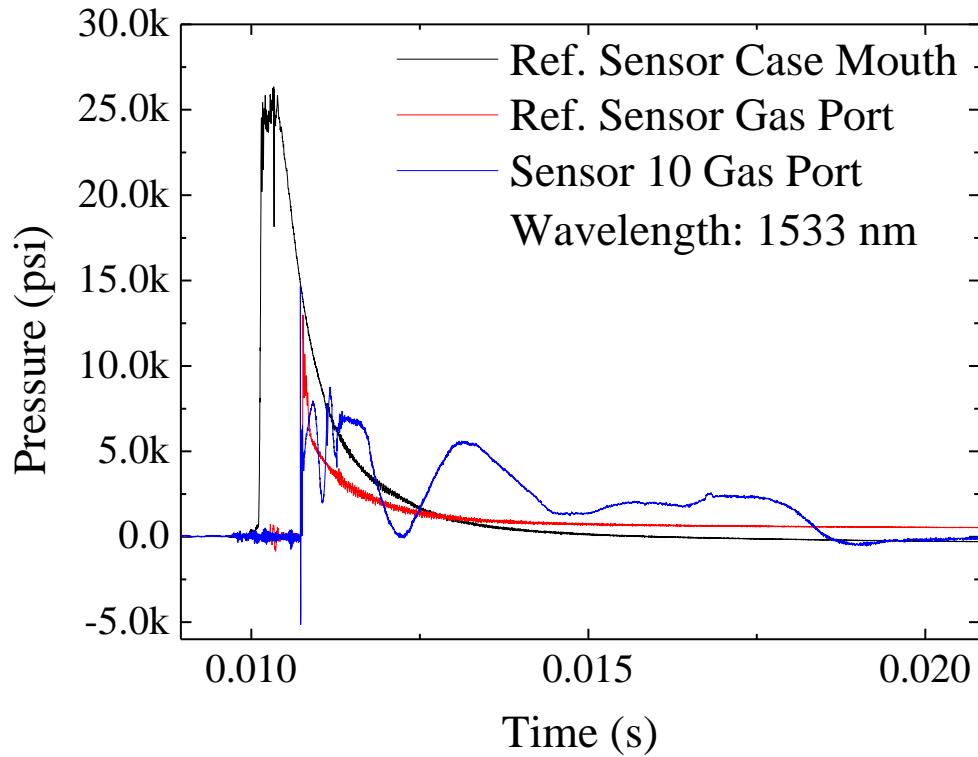
Figure 20: Pressure response from Sensor010 and reference sensors.

The pressure response from Sensor010 is shown in Fig. 20. The sensor was mounted at gas port. It can be seen that the pressure profile follows the profile from the reference sensor. However, an oscillation with a changing period can be seen. This may be caused by the standing wave in the chamber when firing the bullet. The sensor is sensitive enough to pick up the standing wave signals.

Sensor 020:
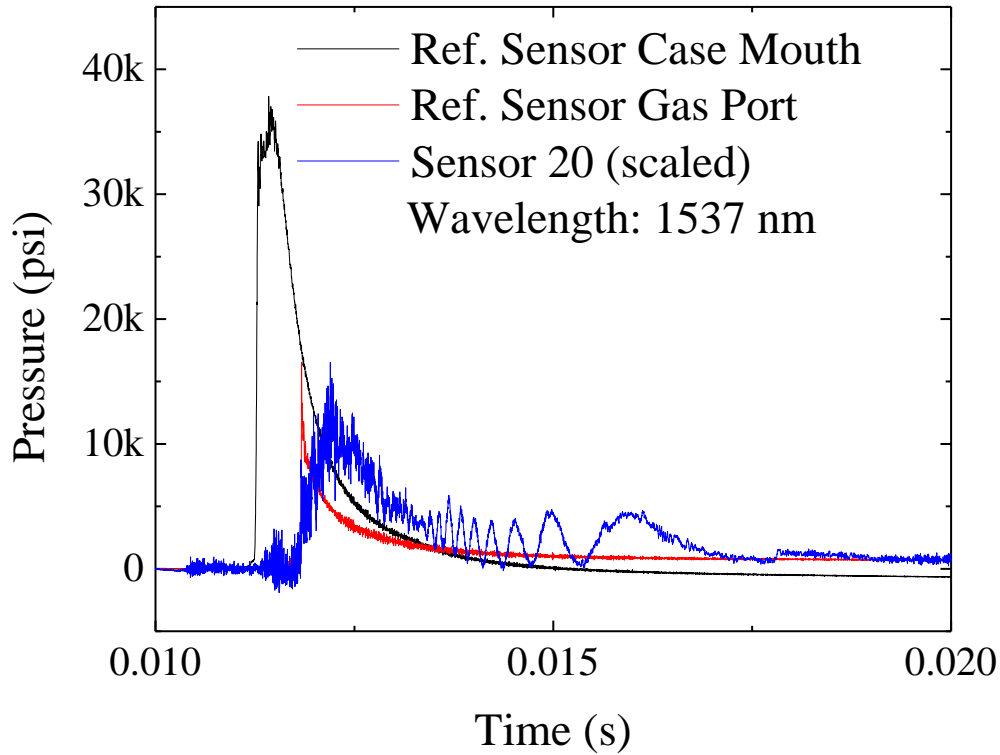
Figure 21: Pressure response from Sensor020 and reference sensors.

The pressure response from Sensor020 is shown in Fig. 21. The sensor was mounted at gas port. It can be seen that the pressure profile follows the profile from the reference sensor. However, an oscillation with a changing period can be seen. This may be caused by the standing wave in the chamber when firing the bullet. The sensor is sensitive enough to pick up the standing wave signals. This was verified by removing an aperture plate in the drift tube and noting that the frequency of the standing was got longer. When the plate was replaced, the frequency shifted back to what is shown above. It is believed that this is the same phenomenon picked up by Sensor 010 and shown in Fig. 20.

Conclusion

Overall, all the sensors have survived the high pressure. The package design appears to work with the high pressures as there were no structural failures, installation was relatively simple and construction was repeatable within the limitations of manual assembly methods. These assembly methods seem to be the root cause of the variability of the sensors' responses. Some sensors' responses follow the profile of the reference sensors and some do not, but these seem to have straightforward causes and it was shown that compensation based on these assumptions resulted in good correlation with the reference sensors. Initial examination of the response and the sensor itself seems to indicate some gas leakage or the diaphragm deflecting more than was expected.

The fact that some of the sensors responded with traces characteristically similar to the reference sensors and those that didn't could be processed, and therefore compensated, based on factors observed on the individual sensor, the experimental results demonstrated that the sensor design is essentially correct and the concept is viable. A signal processing algorithm can successfully demodulate the pressure from the sensor's response even when the sensor's response is out of its working range.

There were a few interesting phenomena observed and the reason why these occurred need to be further analyzed. One of them was the multiple-Fabry Perot (FP)-cavity issue. Due to the similar thickness of the diaphragm and the air cavity, the spectra of sensors show a multi-cavity profile which makes it difficult to distinguish the actual pressure signal. This problem can be addressed by roughening the surface of the diaphragm to destroy the interference condition generated by the diaphragm and leave only the interference spectrum from the air cavity. The ability to catch the standing wave generated by the characteristics of the firing chamber was also interesting. The wave is very visible and illustrates the sensitivity that this design is capable of even in the environment it was operating in.

The main problem observed from these tests was that the sensors' performances were not identical. This can be addressed by improving the manufacture procedure. Future work should center on improving the sensor fabrication procedure so that the sensors can be more robust and their performance can be more consistent.

Appendix A

Sensor Optical Intensity Summary

The following graphs show the intensities at the relevant wavelengths for the sensors used in these tests.

Sensor025 (fixed wavelength at 1545 nm):

Original spectrum versus spectrum after 5 nm (100 kpsi) shift.	Optical intensity output when wavelength is at 1545 nm.
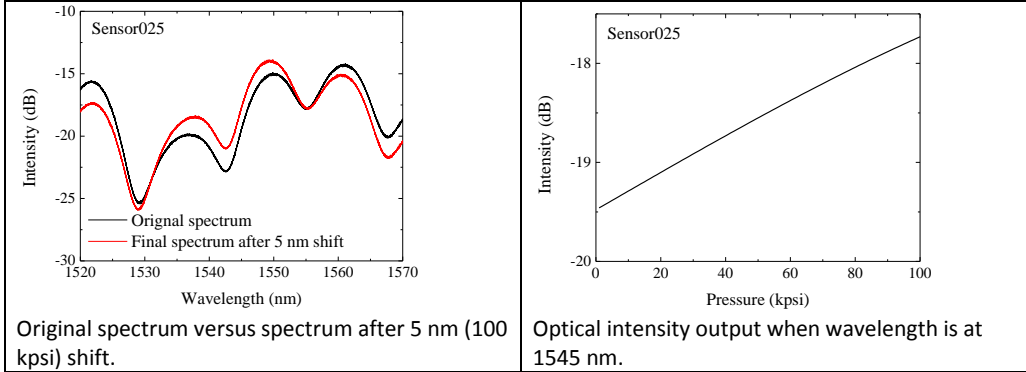
Sensor019 (fixed wavelength at 1528 nm):

Original spectrum versus spectrum after 5 nm (100 kpsi) shift.	Optical intensity output when wavelength is at 1528 nm.
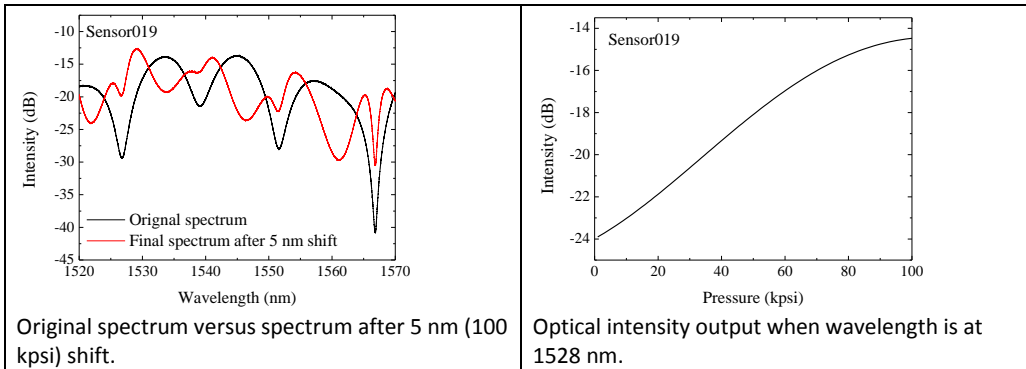
Sensor020 (fixed wavelength at 1552 nm):

20

Original spectrum versus spectrum after 5 nm (100 kpsi) shift.	Optical intensity output when wavelength is at 1552 nm.
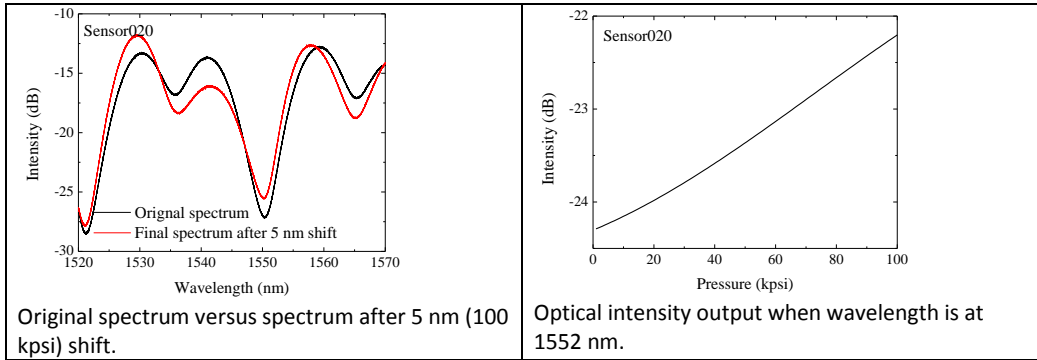
Sensor011 (fixed wavelength at 1522 nm):

Original spectrum versus spectrum after 5 nm (100 kpsi) shift.	Optical intensity output when wavelength is at 1522 nm.
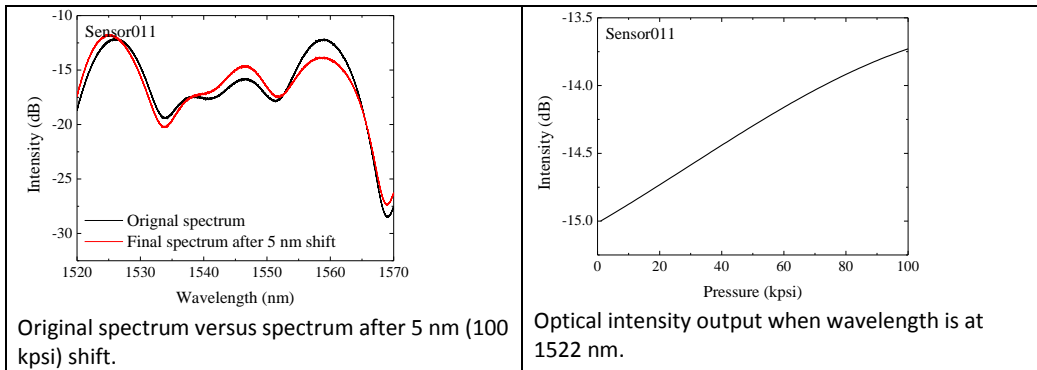
Sensor010 (fixed wavelength at 1534 nm):

Original spectrum versus spectrum after 5 nm (100 kpsi) shift.	Optical intensity output when wavelength is at 1534 nm.